Evaluation method of star sensor's stray light suppression capability through signal-to-noise ratio chain modeling

Wei Yan [1], Jierui Zhang [2]

[1] Beijing Institute of Control Engineering, Beijing 100190, China;

[2] Changchun University of Science and Technology, Changchun 130022, China.

Abstract. To achieve accurate assessment of star sensors' stray light suppression performance, this study develops a novel evaluation approach through integrating ultimate stellar magnitude detection tests with stray light analysis. The proposed methodology employs stellar vector signal-to-noise ratio (SNR) as a direct metric for quantifying stray light resistance. A mathematical framework connecting SNR, point source transmittance (PST), and stellar brightness parameters is formulated through systematic modeling. Experimental validation confirms the validity of using SNR as an evaluation criterion, demonstrating strong correlation between measured values and theoretical predictions. When the stellar SNR exceeds operational detection thresholds, the sensor demonstrates sufficient stray light suppression capacity for detecting celestial objects up to +5.8Mv magnitude. The developed SNR-based evaluation model enables direct assessment of potential stray light interference during orbital operations, providing effective verification of optical system performance and spatial environment compatibility.

Keywords: Stray light inhibition ability; Magnitude; Signal-to-noise ratio; Sunlight suppression Angle; Ground calibration of star sensor.

1. Introduction

Star trackers[1,2], critical for spacecraft attitude determination, require thorough evaluation of stray light suppression via ground verification[3]. Current methods use semi-physical simulations analyzing PST and image grayscale data to assess global/local stray light rejection. PST achieves 10^{-10} precision but relies on external photometric instruments[4,5], limiting in-orbit weak-star validation. Grayscale analysis detects stray light paths with +5Mv[6,7] thresholds but lacks quantitative links between interference and detection limits, leaving performance compliance uncertain[8]. This study introduces an SNR-based framework integrating detection thresholds and stray light mitigation evaluation. It employs physics-driven simulations of optical signals, interference, and noise ratios for comprehensive performance assessment. Validated via a star sensor’s glare suppression system, the method demonstrates effective anti-glare quantification under stray light conditions, addressing prior limitations by correlating interference with measurable magnitude thresholds. This approach has been implemented in practical scenarios through signal-to-noise ratio analysis of a specific star sensor's glare suppression system, successfully demonstrating the effectiveness of the proposed evaluation framework in verifying sensor performance under stray light conditions.

2. Evaluation method of stray light suppression capability based on signal-to-noise link simulation

PST quantifies star trackers' global stray light suppression (off-axis interference resistance), while grayscale data evaluates localized performance, analyzing stray light's impact on target recognition. Validating suppression efficacy ensures reliable in-orbit magnitude detection by minimizing off-axis interference, confirming performance compliance through quantitative detection capability assessments under stray light conditions[9].

2.1 Investigating the linkage between star sensor performance and off-axis stray light interference effects

Star sensors utilize celestial bodies in inertial space as reference points to determine the spacecraft's orientation through the extraction of stellar coordinates from captured star patterns [10]. When operating under optimal conditions, the photoelectric conversion process can be precisely modeled by considering three key factors: the incident stellar radiation intensity, the optical characteristics of the star sensor's components, and the detector's performance parameters [11,12]. This relationship is mathematically expressed in equation (1), which enables systematic calculation of the resultant electrical charge generated during the sensing process.

$$S = N \cdot Q \cdot K = \frac{E_m \cdot \tau_0 \cdot \pi \cdot r^2 \cdot t \cdot Q \cdot K \cdot a^2}{E_{ph} \cdot d^2} \tag{1}$$

Here, Em denotes the incident energy originating from the mMv stellar point. S corresponds to the quantity of signal electrons generated, while N represents the photon count from stellar radiation captured by the optical system during the detector's integration period t. r indicates the Optical aperture radius, τ_0 signifies the system's transmittance efficiency, and d measures the diffraction-induced spot diameter on the detection surface. The parameter a specifies the pixel dimension. Q characterizes the photoelectric conversion's quantum efficiency, and K represents the detector's pixel fill factor coefficient.

When operating in the orbital environment, the sensor encounters not only stellar signal detection but also interference from various stray light sources including solar radiation, earthshine, and lunar illumination. This study specifically examines primary solar interference as a representative case [13,14]. Within the spectral range of $\lambda_1 \sim \lambda_2$, the extraterrestrial solar irradiance incident on the star sensor (Esun) can be calculated using equation (2) as demonstrated in reference [15].

$$E_{sun} = \int_{\lambda_1}^{\lambda_2} k_{mT} \cdot \frac{2\pi hc^2}{\lambda^5 \cdot (e^{\frac{hc}{\lambda kT}} - 1)} d\lambda \tag{2}$$

Where, k_{mT} is the calibration parameter related to apparent magnitude m and color temperature T; λ is the wavelength; h is Planck constant; c is the speed of light in a vacuum; k is the Boltzmann constant.

When the star sensor is exposed to solar radiation at specific incidence angles (α), particular background interference emerges, leading to corresponding electrical charge generation on the detection unit as mathematically represented in equation (3).

$$B = \frac{E_{sun} \cdot \tau_0 \cdot \pi \cdot r^2 \cdot t \cdot Q \cdot \mathrm{K} \cdot a^2}{E_{ph} \cdot f^2} \tag{3}$$

Where, B is the number of noise electrons; f is the focal length of the optical system; $(a/f)^2$ represents the unit pixel solid angle [16].

In the space environment, stray radiation sources emit energy levels typically exceeding the target magnitude by multiple orders of magnitude [17]. Even when attenuated upon entering the star sensor's field of view, these emissions continue to compromise the instrument's magnitude detection capabilities. The signal-to-noise ratio (SNR) serves as a widely accepted metric for evaluating photoelectric system performance under noise-constrained conditions [18-20]. For stellar observation instruments, the criteria necessary for achieving reliable detection of celestial point targets are mathematically defined in equation (4).

$$SNR = \frac{S}{\sqrt{S + B + \sum N_{ele}^2}} \geq V_{th} \tag{4}$$

Where, SNR is the SNR of the star signal; $\sum N_{ele}^2$ is the total number of detector noise electrons; V_{th} is the threshold of SNR to meet certain detection rate and false alarm rate.

The equation reveals that the star signal's signal-to-noise ratio serves as a critical indicator for determining stellar point detection efficacy, while simultaneously demonstrating its dependence on

S, B and $\sum N_{ele}^2$ parameters. Consequently, this analysis enables the identification of correlation linking stellar radiation intensity captured by celestial sensors to ambient stray light exposure levels, thereby facilitating the development of a mathematical framework for assessing stray light suppression capabilities through SNR evaluation metrics.

2.2 A method to evaluate the SNR of star sensor's stray light suppression ability

During orbital operations of a star sensor, the detector simultaneously captures stellar point signals and background irradiation from stray light. Through quantitative analysis, the correlation between the system's Point Source Transmittance (PST), apparent stellar magnitude, and solar irradiation can be mathematically derived using equations (1)-(2), as formalized in equation (5). This parameter represents the residual off-axis stray light energy attenuated by the optical system when the imaging device achieves specified signal-to-noise ratio requirements.

$$PST \leq \frac{E_b}{E_{sun}} = \frac{f^2}{E_{sun}}\left[\frac{\tau_0 \cdot {E_m}^2 \cdot \pi \cdot r^2 \cdot t \cdot Q \cdot K \cdot a^2}{d^4 \cdot E_{ph} \cdot {V_{th}}^2} - \frac{E_m}{d^2} - \frac{E_{ph}\sum N_{ele}^2}{\tau_0 \cdot t \cdot Q \cdot K \cdot \pi \cdot r^2 \cdot a^2}\right] \quad (5)$$

Considering the operational detection process of an orbital star sensor as a case study, the optical configuration demonstrates a focal length of 45mm with 0.9 transmission efficiency. The system operates with 80ms exposure duration and exhibits a diffusion coefficient of 3. The detector employs 5.3μm pixel dimensions coupled with 0.6 visible spectrum photon conversion efficiency. Experimental data reveals that achieving detection probabilities exceeding 99% while maintaining false alarm rates below 1% requires maintaining signal-to-noise ratios above the established 5.0 threshold V_{th} [21]. Fig.1(a) presents comparative theoretical curves illustrating the ultimate detectable magnitudes for various aperture star sensors, with non-physical negative magnitude values intentionally excluded from the visualization.

Star sensors exhibit declining PST as detection thresholds rise, with accelerated attenuation beyond specific magnitudes, leading to negative PST values and upper magnitude limits. Orbital stray light further reduces maximum detectable stellar magnitude. Optimized baffles improve stray light suppression, moderately raising thresholds while lowering PST, but performance remains constrained by optical/detector specifications.

For a 50.0 mm-aperture sensor, Fig.1(a) shows detection thresholds reach +8Mv when PST <3.3 $\times 10^{-7}$. PST evaluations validate compliance with system requirements; exceeding thresholds yields insufficient SNR for star identification. Combined signal/background tests enable direct SNR measurement as a proxy for stray light suppression performance, enabling holistic sensor evaluation.

By establishing correlations between SNR and current assessment frameworks, SNR is proposed as a metric for evaluating stray light suppression capabilities. Through comprehensive analysis of equations (1)-(5), a quantitative linkage emerges connecting SNR with PST parameters, stellar magnitudes, and solar radiation intensity. This analytical connection, derived from fundamental optical principles, achieves mathematical formalization in equation (6), thereby integrating SNR into the evaluation system as a novel diagnostic tool.

$$SNR = \sqrt{\frac{\tau_0 \cdot {E_m}^2 \cdot \pi \cdot r^2 \cdot t \cdot Q \cdot K \cdot a^2}{d^4 \cdot E_{ph} \cdot \left(\frac{PST \cdot E_{sun}}{f^2} + \frac{E_m}{d^2} + \frac{E_{ph}\sum N_{ele}^2}{\tau_0 \cdot t \cdot Q \cdot K \cdot \pi \cdot r^2 \cdot a^2}\right)}} \quad (6)$$

In the range of 5.2E-8≤PST≤1.0E-5, the mathematical relationship between SNR and PST can be obtained according to equation (6). As shown in Fig.1(b), the red vertical marker represents the SNR threshold Vth.

The data demonstrates that at +6.0Mv, the signal-to-noise ratio exceeds the threshold across all PST values, fulfilling star point detection criteria. When observing +7.0Mv, sufficient SNR for stellar extraction occurs only when PST remains below 2.7E-6. For +7.5Mv magnitudes, the threshold requirement is satisfied at PST levels under 8.5E-7. The +8.0Mv condition maintains adequate SNR for star identification exclusively when PST stays beneath 2.7E-7. Conversely,

+8.5Mv observations show SNR consistently below the critical threshold throughout the tested PST range, rendering star extraction unfeasible under these parameters.

This study examines the correlation between detection threshold magnitudes and PST values under a 50.0mm aperture condition, as visualized through comparative analysis with Fig.1(a). Fig.1(c) displays these findings, with the red-highlighted section illustrating the Mv-PST correlation across the PST spectrum presented in Fig.1(a). Additionally, the diagram specifies the PST thresholds required for different magnitude detection levels. A strong consistency emerges between the outcomes illustrated in Fig.1(b) and those presented in Fig.1(c).

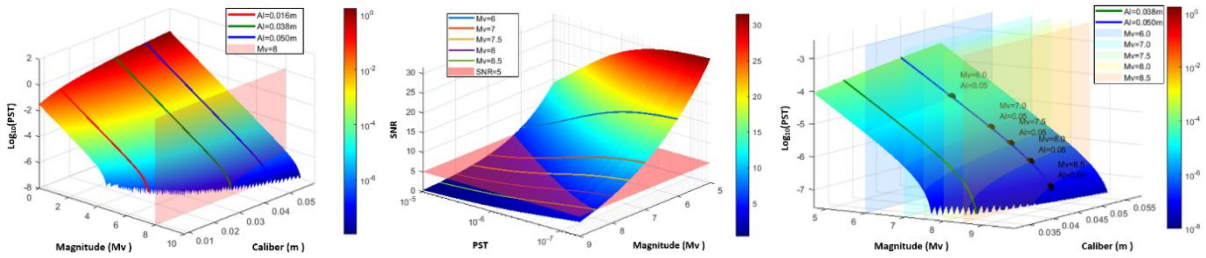

Fig. 1 Relationship between limit detection magnitude, PST and SNR
(a) Relationship between limit detection magnitude and PST at different calibers
(b) Relationship between SNR and PST at different limit detection magnitudes
(c) Correspondence between time magnitude and PST when detection conditions are met

SNR/PST interdependence underpins star sensor evaluations, linking stray light suppression to detection magnitude thresholds. By comparing measured SNR against criteria, engineers validate anti-interference performance, enabling integrated assessment of detection limits and light mitigation efficacy via theoretical frameworks.

3. The overall composition and working principle of the signal and noise link test system for star sensor's stray light suppression capability

The necessary condition to realize the imaging test of starlight vector of star sensor under the interference of off-axis space solar irradiation is to simulate the navigation target and the possible off-axis stray light interference of star sensor in orbit. The function and main composition of signal-noise link test system are analyzed.

The signal and noise link test system for star sensor's stray light suppression ability mainly consists of space solar irradiation simulation system, starlight vector simulation system and solar incidence Angle simulation turntable, as shown in Fig.2. According to the signal-to-noise link test method, the main functions of the components of the test system are analyzed.

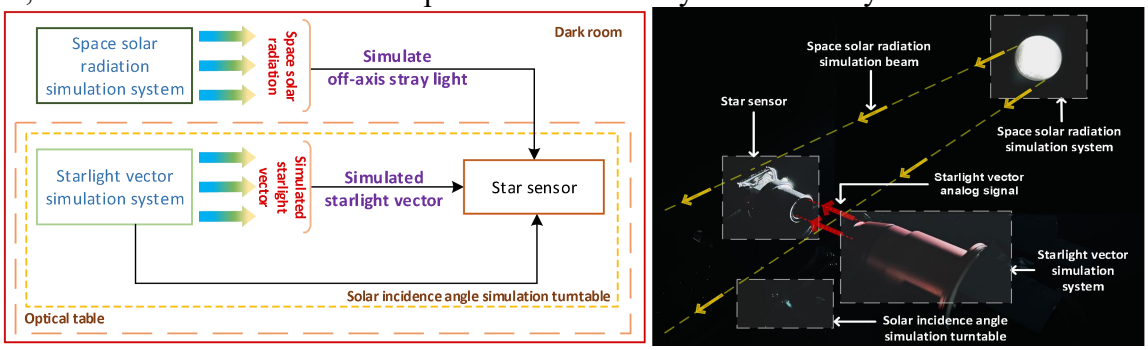

Fig. 2 Signal and noise link test system for star sensor's stray light suppression capability

The sensor subsequently captures both stellar signals and stray light patterns, enabling quantitative analysis of grayscale characteristics in stray background and stellar images across varying solar incidence angles. Stray light suppression capability was quantified using signal-to-noise ratio metrics (SNR threshold Vth≥5) as evaluation criteria.

4. Test of stray light suppression capability of a star sensor based on signal-to-noise link simulation

SNR measurement system integrates solar simulators (35°–90° angles), starlight vectors (+4Mv), and angle adjustment platforms to evaluate stray light rejection. Testing involved +5Mv/5.8Mv targets under three trials per condition; the sensor successfully imaged +5.8Mv stars at 28°–50° solar angles, validating performance, as shown in Fig.3.

The 3×3 pixel region containing the target is selected in the gray distribution of the starlight vector, and the gray mean S of the starlight vector is calculated. Outside this region, 9×9 pixel region is selected to calculate background gray mean N, and background gray mean square error Nstd, then the measured SNR of starlight vector can be calculated by equation (7). Thus, the mean of measured SNR line chart of three repeated tests was obtained, as shown in Fig.3(f).

$$SNR = \frac{S-N}{N_{std}} \tag{7}$$

At the same time, measurement uncertainty serves as a statistical indicator quantifying the variability observed in measurement outcomes, demonstrating the reliability of obtained data. For SNR measurement uncertainty determination, the Class A assessment approach is implemented. Considering the starlight vector's SNR calculation derives from the mean of three independent measurements, the following parameters must be acquired.

Average SNR value $\overline{SNR}$ obtained through n separate experimental trials. The standard deviation of the SNR $s(SNR_i)$ calculated from an individual measurement. Finally, the standard uncertainty u can be found in equation (8).

$$u = s(SNR_i) = \sqrt{\frac{1}{n-1}\sum_{i=1}^{n}(SNR_i - \overline{SNR})^2} = \sqrt{\frac{1}{n-1}\sum_{i=1}^{n}\left(SNR_i - \frac{1}{n}\sum_{i=1}^{n}SNR_i\right)^2} \tag{8}$$

Therefore, the SNR measurement uncertainty becomes quantifiable, enabling the derivation of how the star sensor's starlight vector measurement uncertainty changes relative to spatial solar radiation's incident angle, as depicted in Fig.3(f) as well.

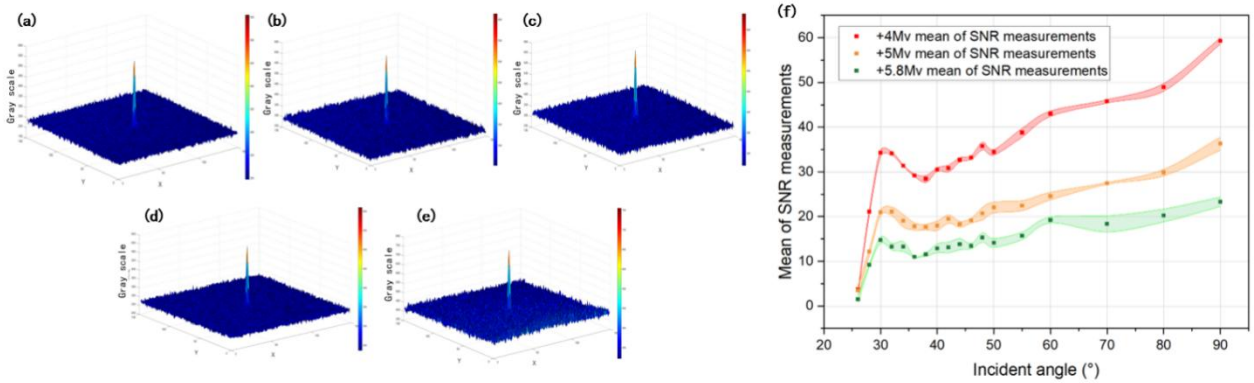

Fig.3 +5.8Mv stellar vector gray scale and multiple measurements
(a) 50° grayscale (b) 40° grayscale (c) 36° grayscale (d) 30° grayscale (e) 28° grayscale
(f) relationship between starlight vector SNR measured by different magnitudes

Star tracker experiments reveal that decreasing solar angles intensify background luminance and reduce SNR; below 40°, stray light infiltration causes exponential noise growth, plummeting SNR <5. Above 40°, baffles stabilize measurements. Tests show SNR variability <2.0 across detection magnitudes, confirming compliance with stray light suppression criteria.

5. Summary

This study introduces a novel assessment approach for evaluating stray light suppression capabilities in star sensors. By employing a SNR-based evaluation framework within a star vector simulation system, the methodology quantifies optical interference resistance performance while visually demonstrating the sensor's capacity to mitigate extraneous light sources beyond its

operational field of view during orbital missions. The experimental configuration incorporates devices such as spatial solar radiation simulation apparatus, stellar vector emulation systems, and solar incidence angle simulation components, achieving physical simulation verification of stray light suppression with a detection threshold of +5.8Mv. The validation of the SNR assessment model confirms its effectiveness in evaluating optical interference resistance, establishing critical references for optimizing solar exclusion angles in orbital operations. This methodology simultaneously validates the optical characteristics and spatial environment compatibility of star sensors, thereby enhancing operational reliability assurance for spaceborne applications.

References

[1] T. E. Strikwerda, H. L. Fisher, C. C. Kilgus, L. J. Frank, Autonomous star identification and spacecraft attitude determination with CCD star trackers. Spacecraft Guidance, Navigation and Control Systems, (1991) 195-200.

[2] J. Lu, C. Lei, Y. Yang, A dynamic precision evaluation method for the star sensor in the stellar-inertial navigation system. Scientific Reports, 7(1), (2017) 4356.

[3] H. Kawano, Y. Sato, K. Mitani, H. Kanai, K. Hama, New light-shielding technique for shortening the baffle length of a star sensor, Proceedings of SPIE - The International Society for Optical Engineering, 80(3), (2002) 249-249.

[4] R. P. Heinisch, C. L. Jolliffe, Light baffle attenuation measurements in the visible, Applied Optics, 10(9), (1971) 2016-20.

[5] L. Xu, Research on key technologies of stray light measurement for large aperture optical system, Xi'an Institute of Optics and precision machinery, Chinese Academy of Sciences, (2019).

[6] H. Kawano, L. Mazuray, R. Wartmann, H. Shimoji, S. Yoshikawa, K. Miyatake, et al, Suppression of sun interference in the star sensor baffling stray light by total internal reflection. Proceedings of SPIE - The International Society for Optical Engineering, 5962, (2005) 59621R-59621R-10.

[7] S. Lee, R. Saleem, S. S. Lee, A micro star tracker with curved vane for short baffle length and sharp stray light attenuation. Applied Optics, 59(13), (2020).

[8] Z. Du, L. Zhang, H. Chen, X. Si, W. Xu, H. Liu, et al, Design of on-orbit Lighting environment simulation system for space optical remote sensor, Acta Photonica Sinica, 46(10), (2017) 8.

[9] M. Marciniak, J. Enright, D. Sinclair, T. Dzamba, Microsatellite star tracker baffles: validation and testing. (2013)

[10] C. C. Liebe, Accuracy performance of star trackers - a tutorial, IEEE Transactions on Aerospace Electronic Systems, 38(2), (2002) 587-599.

[11] X. Zhong, J. Jia, G. Jin, H. Qu, G. Liu, Detecting performance and overall design of airborne daytime star sensor for navigation, Optics and Precision Engineering, 19(12), (2011) 2900-2906.

[12] Y. Pan, H. Wang, N. Jing, Y. Shen, Y. Xue, J. Liu, et al, Parameter selection and optical design of all-day star sensor, Acta Photonica Sinica, 45(1), (2016).

[13] H. Wang, W. Hua, H. Xu, Y. Xu,. Centroiding Method for Star Image Spots under Interference of Sun Stray light Noise in a Star Sensor. Acta Optica Sinica, 41(3), (2021) 0312005.

[14] Z. You, Space Microsystems and Micro/Nano Satellites, (2017).

[15] Y. Pan, H. Wang, N. Jing, Y. Shen, Y. Xue, J. Liu, et al, Parameter selection and optical design of all-day star sensor, Acta Photonica Sinica, 45(1), (2016).

[16] B. Ren, G. Jin, T. Wang, X. Zhong, P. Zhang, Parameter design and experiment of airborne all-sky star sensor, Infrared and Laser Engineering, 42(4), (2013) 1003-1010.

[17] Y. Wu,. The design of a special type hood based on the sun synchronous orbit satellite star sensor, Proceedings of the 2013 Symposium on Space Optics and Mechatronics, Chinese Society for Space Science, (2013).

[18] W. Zhang, W. Quan, Detection capability analysis of CMOS Star sensor under high dynamic condition, 7th Annual Conference of Deep Space Exploration Technology Committee of Chinese Society of Astronautics, (2012).

[19] J. Yuan, J. Zhang, Study on detection sensitivity of navigation star sensor. OPTO-ELECTRONIC ENGINEERING, 26(6), (1999) 6.

[20] M. Elbaum, P. Diament, Snr in photocounting images of rough objects in partially coherent light. Applied Optics, 15(9), (1976) 2268.

[21] Radio Company (USA), Electrooptics Manual (National Defence Industry, 1978) (in Chinese).